PHILOSOPHICAL MAGAZINE A, 1988, VOL. 57, NO. 6, 955–969

A high-resolution transmission electron microscopy investigation of the δ'–θ' precipitate structure in an Al–2 wt% Li–1 wt% Cu alloy

By J. M. HOWE and D. E. LAUGHLIN

Department of Metallurgical Engineering and Materials Science, Carnegie Mellon University, Pittsburgh, Pennsylvania 15213, U.S.A.

and A. K. VASUDÉVAN

Alcoa Technical Center, Aluminium Company of America, Alcoa Center, Pennsylvania 15069, U.S.A.

[*Received 1 September 1987 and accepted 7 October 1987*]

ABSTRACT

High-resolution transmission electron microscopy was used to investigate the atomic structure of the two-phase δ'–θ' precipitate which forms in Al–Li–Cu alloys. The results show that θ' plates often thicken in multiples of two unit cells and that the interphase boundary at the plate faces is atomically flat and coherent with the surrounding δ' phase. The positions of Cu atoms in the top half and bottom half of the θ' unit cell causes the ordered δ' phase to form in an antiphase relationship on opposite faces of the θ' precipitate. This antiphase relation is continued into the δ' beyond the plate edge, which is largely coherent, forming an antiphase boundary. These observations are explained in terms of conservative mechanisms of precipitate growth involving $(a/2)[100]$ and $(a/2)[010]$ transformation dislocations and bonding tendencies among Al, Li and Cu atoms.

§ 1. INTRODUCTION

Extensive investigation of Al–Li–Cu alloys is currently in progress because the high strength-to-weight ratio of these alloys makes them attractive candidates for aerospace applications (Sanders and Starke 1981, 1984, Baker, Gregson, Harris and Peel 1986). In most Al–Li–Cu alloys, a two-phase precipitate structure, consisting of a thin plate-shaped semicoherent θ' phase that is coated with a coherent δ' phase forms on the $\{100\}$ matrix planes during ageing (Rioja and Ludwiczak 1986, Tosten, Vasudévan and Howell 1986, 1988). Although this is a common phase in these alloys, the reason for the formation of the two-phase structure, which is peculiar to Al–Li-base alloys, is not known.

The crystal structures of the individual θ' and δ' phases are well established (Silcock, Heal and Hardy 1953–4, Silcock 1959–60) and are illustrated in fig. 1. The plate-shaped θ' phase has a b.c.t. crystal structure (point group 4/mmm) with the composition Al_2Cu, as shown by the unit cell in fig. 1 (*a*). Of particular importance in this structure is the fact that the vertical axes passing through the corners of the unit cell in fig. 1 (*a*) are not the fourfold axes, they are fourfold rotary-inversion axes. The fourfold vertical axes pass through the Cu atoms. The structure could be redrawn to have the fourfold axes go through the corners of the unit cell, making the space group I4/mmm more apparent. The δ' phase that coats the θ' phase has an $L1_2$ ordered

Fig. 1

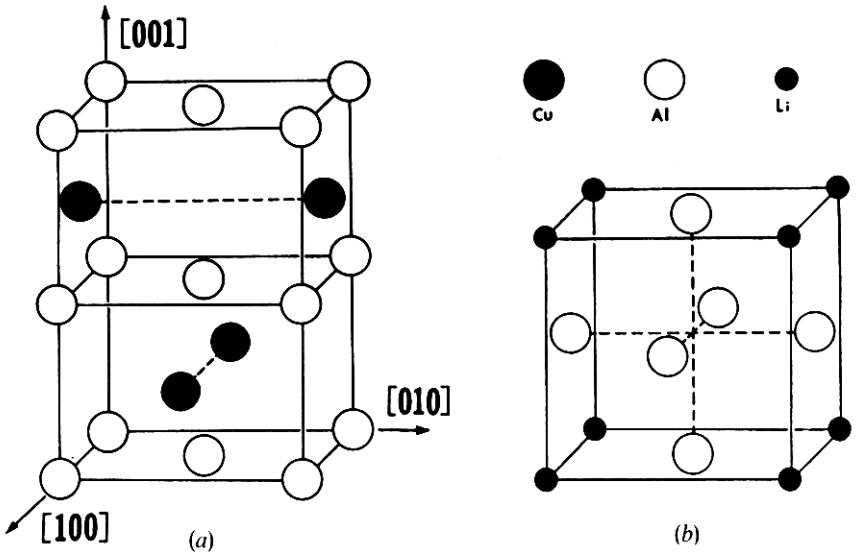

Atomic arrangements within (a) the b.c.t. θ' unit cell and (*b*) the cubic $L1_2$ unit cell.

structure (point group m3m) with the composition Al_3Li, as shown by the unit cell in fig. 1 (*b*). The δ' phase usually forms as coherent spherical precipitates in binary Al–Li alloys (Noble and Thompson 1971, Williams and Howell 1988), while the θ' structure forms as semicoherent plate-shaped precipitates on the {100} planes in Al–Cu binary alloys with the orientation relationship $\{001\}_\alpha \| \{001\}_{\theta'}$ and $\langle 100\rangle_\alpha \| \langle 100\rangle_{\theta'}$ (Silcock 1953–4, Mondolfo 1979). Both phases impart significant strength to the Al matrix and there has been considerable interest in understanding their mechanisms of growth and strengthening (Glazer, Edgecumbe and Morris 1986, Huang and Ardell 1986).

In this investigation, high-resolution transmission electron microscopy (HRTEM) was used to examine the internal and interfacial structures of the δ' and θ' phases in an Al–Li–Cu alloys, in order to understand the mechanisms responsible for the development of this two-phase precipitate morphology. The results from a complementary investigation on the deformation mechanisms of these precipitates will be presented elsewhere (Howe and Vasudévan 1988).

§2. Experimental procedures

The composition of the lab-fabricated alloy used in this study is shown below. The alloy was homogenized and fabricated in the form of 12 mm plate by Alcoa. The plate was solution annealed for 30 min at 550°C, quenched in cold water and aged for 32 h at 190°C, to near the peak strength condition (A. K. Vasudévan 1986, unpublished work). Thin foils were prepared for HRTEM by cutting slices on a diamond saw, punching 3·0 mm discs from the slices and electropolishing in a twin-jet Fischione apparatus using a 20% HNO_3–methanol electrolyte at −40°C, 15 V and 12 mA. After perforation, samples were rinsed in methanol and stored in ethanol until examination. Thin foils were examined on the Berkeley JEOL ARM1000 operating at 800 keV with an undersaturated LaB_6 filament. Through-focus series of images were taken in a $\langle 100\rangle_\alpha$

Al-rich matrix zone axis using a $6{\cdot}5\,nm^{-1}$ radius objective aperture and focus increments of 3·0 nm. Simulated HRTEM images were calculated using the SHRLI multislice programs (Cowley and Moodie 1957, O'Keefe and Buseck 1979) with all reflections to $40{\cdot}0\,nm^{-1}$ included in the calculations. The microscope parameters used for the JEOL ARM1000 in the simulations were $C_s = 2{\cdot}4$ mm, $\alpha = 1{\cdot}0$ mrad, $\Delta = 5$ nm and $\Delta f_{Scherzer} = -60{\cdot}0$ nm.

Chemical composition of experimental Al–Li–Cu alloy.

Element	Li	Cu	Fe	Si	Al
Amount (wt %)	2·1	1·3	0·05	0·03	Balance

§ 3. Experimental results and discussion

3.1. *High-resolution transmission electron microscopy of the δ′–θ′ interface*

An example of the two-phase δ'–θ' precipitate structure is shown in the transmission electron microscopy (TEM) image in fig. 2 (*a*), which is a dark-field image formed using a 010 δ' precipitate reflection in a $\langle 100\rangle_{\delta'} \| \langle 100\rangle_{\theta'}$ orientation. In this image, the bright δ' phase forms irregular-shaped but continuous layers about 20 nm thick along the

Fig. 2

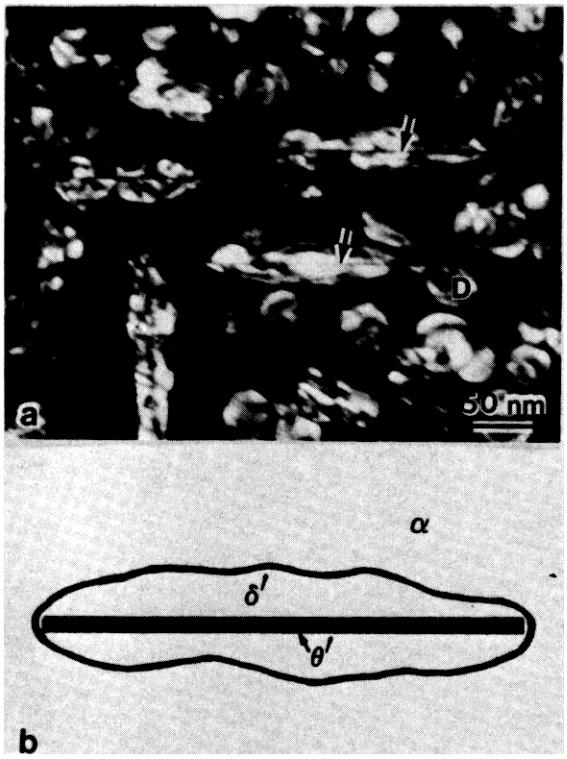

(*a*) Dark-field TEM image of δ'–θ' two-phase precipitates in a $\langle 100\rangle_{\delta'} \| \langle 100\rangle_{\theta'}$ orientation using a 010 δ' reflection; (*b*) illustration of the two-phase precipitate structure.

faces of the θ' plates, which are visible as dark lines (arrows) in the centres of the δ'. The δ' phase does not appear to grow around the edges of the θ' plates to the thickness that it achieves on the faces, and the resulting two-phase precipitate structure has the overall morphology sketched in fig. 2(*b*). Additional spherical δ' precipitates are visible throughout the matrix in fig. 2(*a*).

An HRTEM image of the δ'–θ' precipitate structure in a $\langle 100 \rangle_a$ orientation is shown in fig. 3. In this image, the θ' precipitate plate which is edge on and darker than the δ' surrounding it, is about 1·2 nm thick and 80 nm in diameter (the left-hand end of

Fig. 3

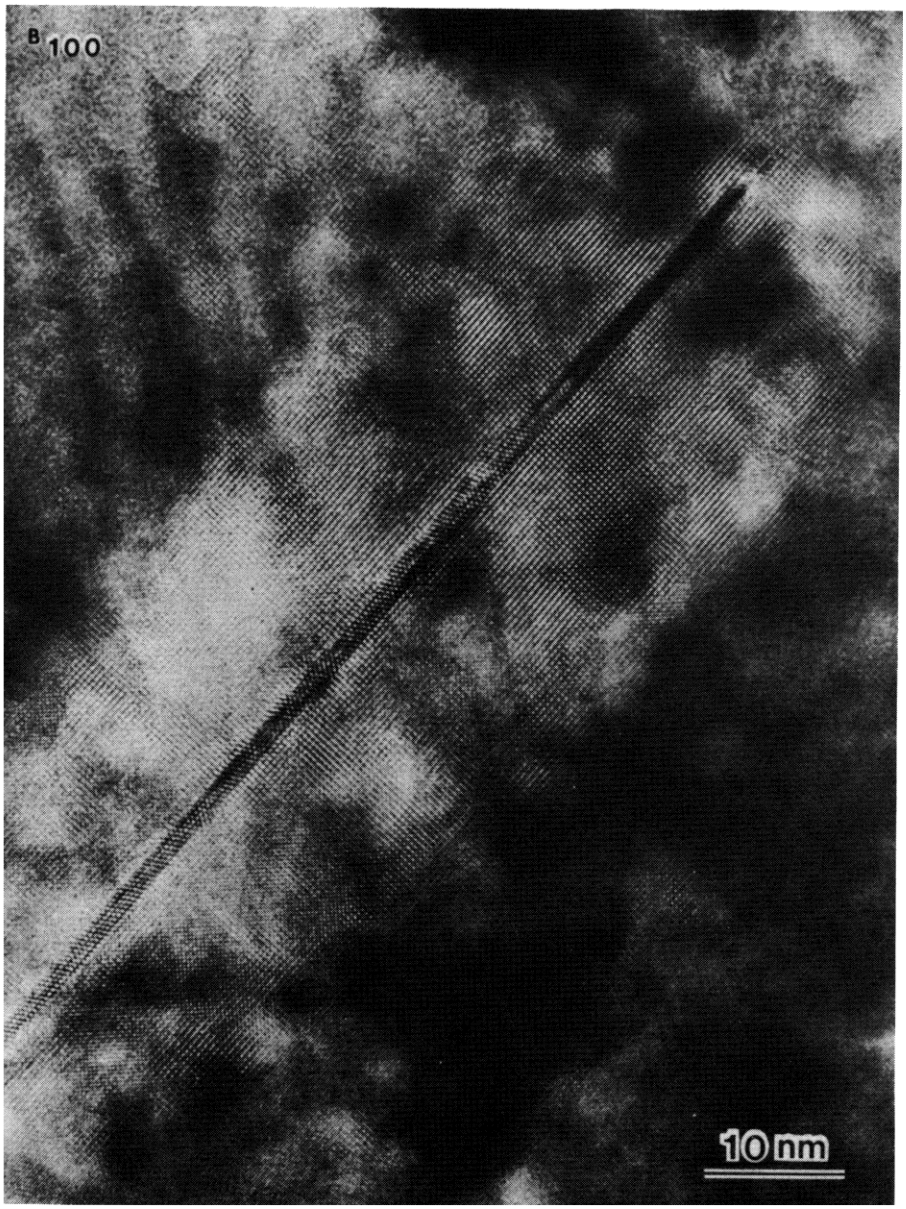

HRTEM image of the δ'–θ' precipitate structure in a $\langle 100 \rangle_a$ orientation.

the precipitate is just off the micrograph, at the edge of the hole). The δ' coating which is lighter than either the θ' plate or the Al-rich matrix, is about 16 nm thick on the plate faces and appears just to envelop the plate edge. The δ'–θ' interphase boundary appears atomically sharp and flat on both faces of the θ' plate, while the α–δ' interface is somewhat diffuse and rough. These features are clearer in the enlargement of the central region, shown in fig. 4.

In fig. 4, the 0·2 nm {200} planes of the Al-rich α phase are visible at the top and bottom of the micrograph, and the δ' phase is distinguished by the strong contrast of {100} planes (alternate {200} planes) due to the ordered $L1_2$ structure with a spacing of

Fig. 4

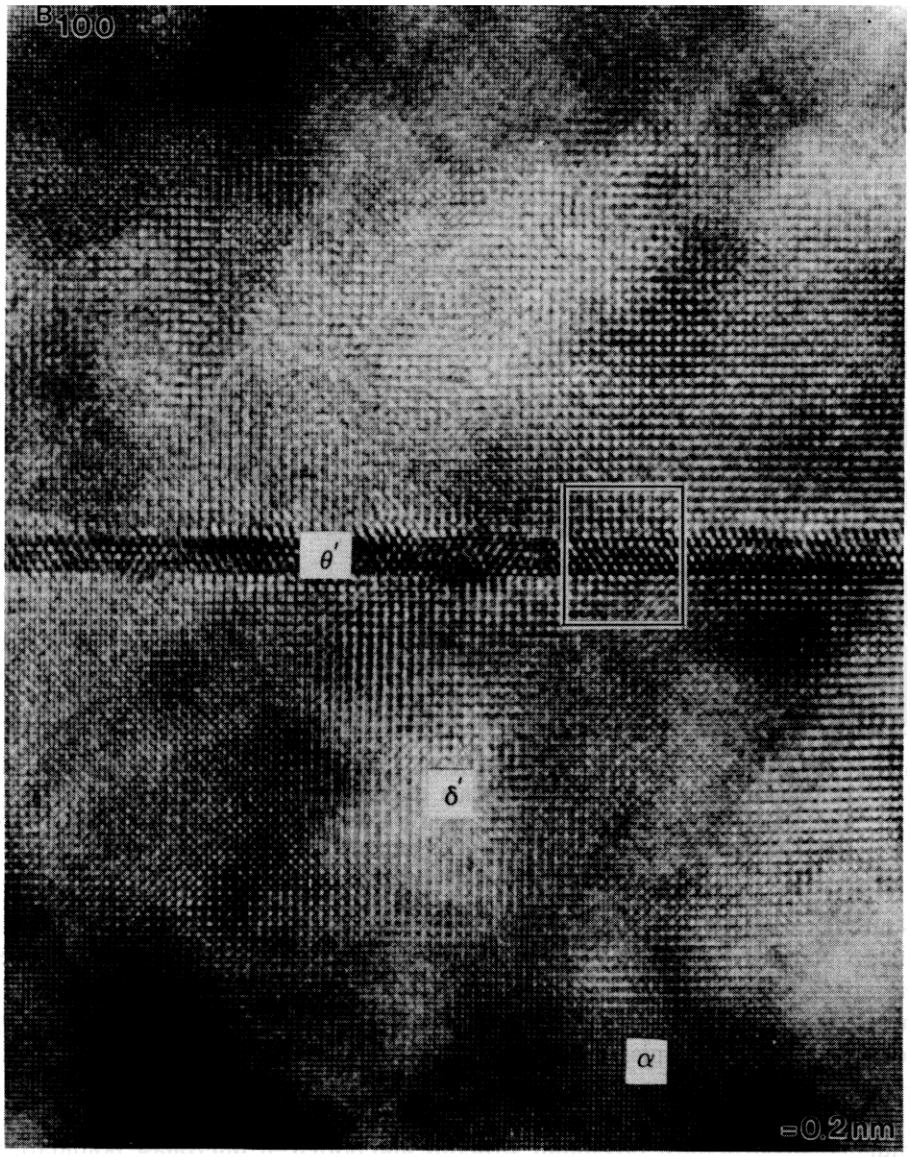

Enlargement showing the structures of the δ'–θ' and α–δ' interphase boundaries.

Fig. 5

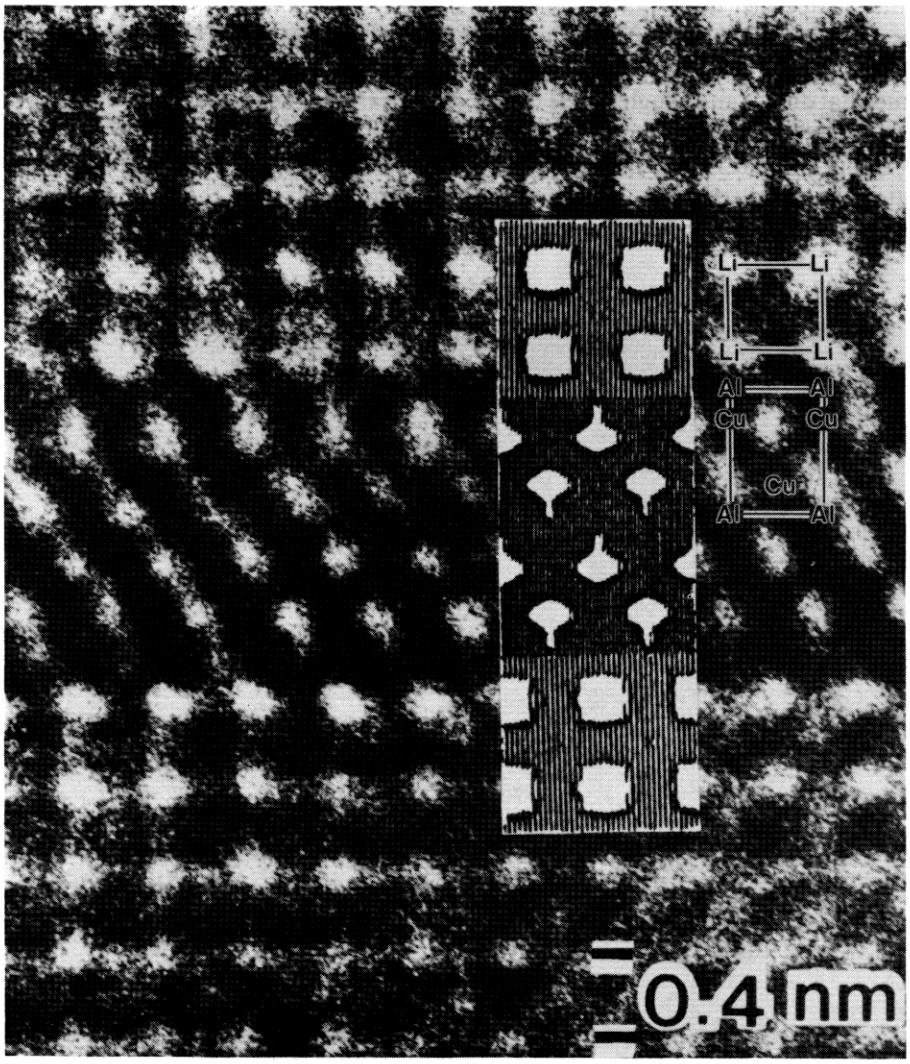

Enlargement of the area enclosed near the centre of fig. 4 with a simulated HRTEM image of the two-phase precipitate structure at 4 nm thickness and Scherzer defocus (−60·0 nm) superimposed. The positions of Al, Li and Cu atoms in the δ' and θ' unit cells are shown superimposed on the experimental image, adjacent to the simulated image.

0·4 nm. The irregularity of the α–δ' interface is evident by the uneven termination of the $\{100\}$ δ' planes in the Al-rich α matrix phase, and the coherency of the α–δ' interface is also apparent by the complete matching of the $\{200\}$ planes between the α and δ' phases. The planarity of the δ'–θ' interphase boundary is also evident in fig. 4, although the matching of crystal planes across this interface is not as straightforward as at the α–δ' interphase boundary.

Figure 5 shows a further enlargement of the area enclosed near the centre of fig. 4. A simulated image of the θ' precipitate structure and both δ'–θ' interphase boundaries is shown superimposed on the experimental image. The matching between the

experimental and simulated images for both the δ' and θ' precipitate structures as well as at the δ'–θ' interphase boundary at the same specimen thickness and defocus verifies that the atomic structures used as initial input for the image simulations are correct. This structure, seen as the projected specimen potential along a $\langle 100\rangle_{\delta'} \| \langle 100\rangle_{\theta'}$ direction, is shown in fig. 6 (*a*) and the unit cells of the δ' and θ' structures are outlined in fig. 6 (*a*), as well as adjacent to the simulated image in fig. 5, for comparison with the unit cells shown in figs. 1 (*a*) and (*b*). The corresponding simulated image previously shown superimposed on fig. 5 is also shown in fig. 6 (*b*), for comparison with the projected specimen potential.

Examination of the projected potential for δ' in fig. 6 (*a*) and the simulated image in fig. 6 (*b*) indicates that Li atom positions in the δ' structure appear bright because Li is a weak scatterer of electrons, while Al atom positions appear dark since Al is a comparatively strong scatterer of electrons (Hirsch, Howie, Nicholson, Pashley and Whelan 1977). In the θ' structure, both Al and Cu atoms scatter electrons strongly, causing them to appear dark, while electrons travelling through relatively open regions in the θ' structure lead to asymmetric bright spots among the Cu and Al atoms. Thus, both the δ' and the θ' phases appear to be weak-phase objects for 800 keV electrons at this specimen thickness and microscope (Scherzer) defocus, i.e., the atom positions are dark on a bright background and there is a linear relation between the darkness of the atom positions and the projected specimen potential (Spence 1981, O'Keefe 1984).

3.2. *Mechanisms of θ' growth*

Knowing the atomic arrangements within the δ' and θ' precipitates and across the δ'–θ' interphase boundary reveals several interesting features about the mechanisms of growth of this two-phase structure. First, the θ' precipitate plate is two unit cells thick (1·16 nm) and the interphase boundary is atomically flat on both sides. Previous analyses of the structure of θ' plates in Al–Cu alloys (Stobbs and Purdy 1978, Dahmen and Westmacott 1983) have shown that growth occurs in discrete steps in order to minimize both the shape and the volume changes associated with the transformation. Two simple criteria followed during growth are:

(1) growth ledges occur in pairs of opposite shears to accommodate the shape change in the f.c.c.→b.c.t. transformation and
(2) conservative and non-conservative building units of θ' form in certain combinations to reduce the volume strain in the transformation, which in this case lies along the *c*-direction.

The smallest unit cell allowed by these criteria is a conservative precipitate two unit cells thick, with a −0·052 nm contraction along ⟨001⟩. The θ' precipitate in fig. 5 is exactly two unit cells thick, supporting this theory of growth. The above criteria further predict that the next growth step will be a pair of conservative–non-conservative shears with an expansion of +0·062 nm along ⟨001⟩. This counters the −0·052 nm contraction, leaving a total expansion of +0·01 nm, corresponding to an interstitial strain of 0·5% and a precipitate which is 3·5 θ' unit cells thick. Further growth should proceed by another conservative pair bringing the thickness to 5·5 θ' unit cells and a vacancy strain field, followed by another conservative–non-conservative pair, and so on. While the previous investigators (Stobbs and Purdy 1978, Dakmen and Westmacott 1983) found good agreement for

Fig. 6

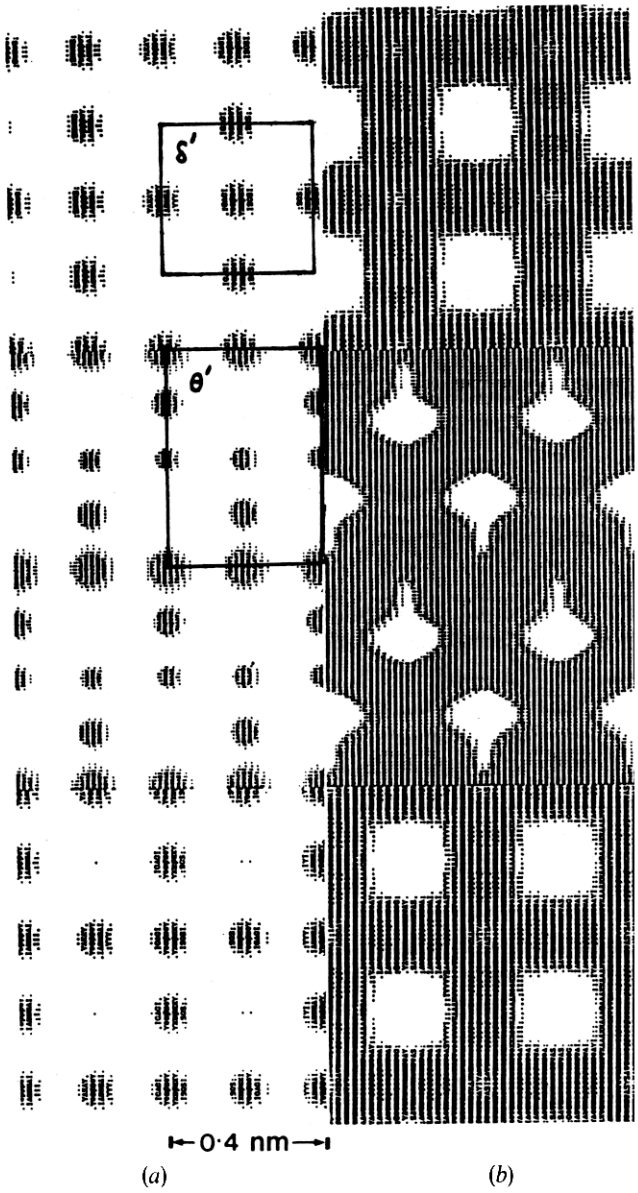

(*a*) Projected specimen potential for the two-phase precipitate with the δ' and θ' unit cells indicated: (*b*) corresponding simulated image at 4 nm thickness and Scherzer defocus (−60·0 nm).

this sequence of growth in Al–Cu alloys, the θ' precipitates observed in this study usually contained an integral number of unit cells, as demonstrated by the θ' precipitate plates, which are two, three and four unit cells thick in fig. 7. Although the reason for this difference may be due to strains caused by the surrounding δ' phase, simple calculations considering the $-0{\cdot}03$ nm contraction along $\langle 001 \rangle$ in δ' and the conservative and non-conservative building units proposed previously fail to account for the integral unit-cell combinations observed in this system.

3.3. *Mechanisms of δ' growth*

Another important observation from fig. 5 is that the δ' phase on the top face of the θ' plate is translated exactly one-half of the unit-cell dimension (0·2 nm) with respect to the δ' phase on the bottom face of the precipitate, i.e. Li atoms (bright) on one side of the θ' precipitate are aligned with Al atoms (dark) on the opposite side. This forms an antiphase boundary (APB) in the δ' phase across the precipitate, and the same feature is observed for the precipitates two, three and four unit cells thick shown in fig. 7. In addition, the δ' appears to form such that Li atoms are adjacent to Cu atoms in the θ'

Fig. 7

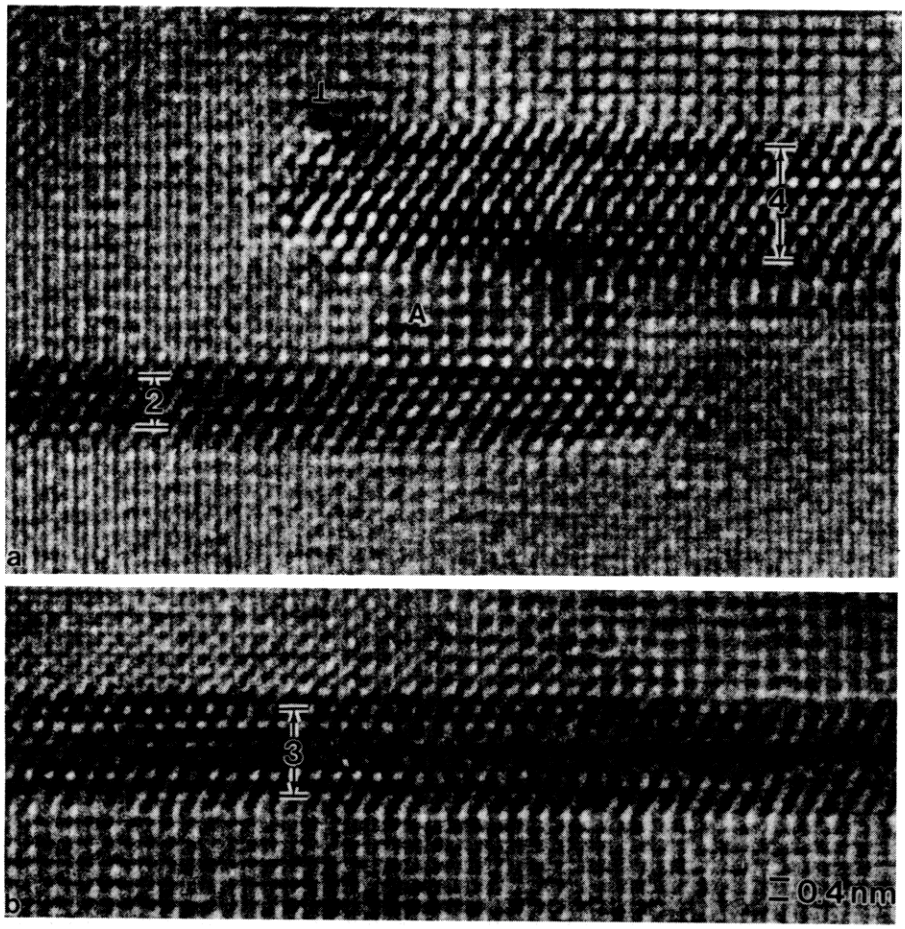

(*a*) Two and four unit cell θ' precipitate plates with APBs between δ' on opposite faces; (*b*) three unit cell θ' precipitate with an APB between δ' on opposite faces.

phase, as seen by comparing the positions of Li and Cu atoms in the projected potential in fig. 6 (*a*) and also by inspection of the unit cells for δ' and θ' adjacent to the simulated HRTEM image in fig. 5.

The reason for the alignment of Li and Cu atoms across the δ'–θ' interface can be explained by considering mechanisms of epitaxial growth of the δ' phase on a pre-existing θ' plate, and by comparing bond energies among Al, Li and Cu atoms. A $\langle 001 \rangle$ projection of the top surface in the θ' unit cell in fig. 1 (*a*) is shown in fig. 8 (*a*), with the positions of Cu atoms on the left- and right-hand faces in the top half of the unit cell also indicated. A $\langle 001 \rangle$ projection of the bottom surface in the δ' unit cell in fig. 1 (*b*) is shown in fig. 8 (*b*). When the δ' phase grows on the surface of θ', the Al atoms in the centres of the δ' and θ' faces will not lie opposite one another because this is not a favourable packing situation. Therefore the Li atoms at the corners of the δ' unit cell can lie in either of two positions on the surface of the θ'; these are enclosed by broken lines and labelled A and B in fig. 8 (*a*). If the Li atoms reside in position A, Al atoms in the δ' lie above Cu atoms in the θ' as illustrated in fig. 8 (*c*) while, if the Li atoms reside in position B, Li atoms in the δ' lie above Cu atoms in the θ' as illustrated in fig. 8 (*d*). In both cases the nearest-neighbour bonds for the Li and Al atoms in δ' are four Al atoms, and whether configuration A or B is more favourable is determined by whether Li or Al is more strongly bound to the Cu atoms just beneath the surface in θ'. All the previous HRTEM images have shown that the Li atoms in δ' lie across from Cu atoms in θ' and that configuration B in fig. 8 (*d*) occurs.

Fig. 8

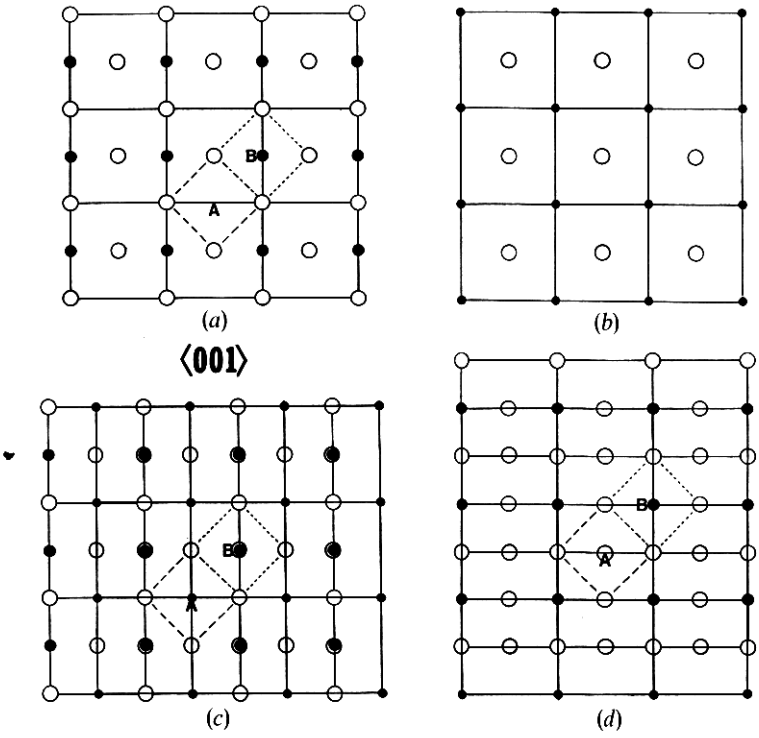

(*a*) A $\langle 001 \rangle$ projection of the top surface of the θ' unit cell with the nearest-neighbour Cu atoms also shown; (*b*) a $\langle 001 \rangle$ projection of the bottom surface of the δ' unit cell; (*c*) the θ' unit cell in (*b*) superimposed on the δ' unit cell in (*a*) with Li atoms in position A; (*d*) the θ' unit cell in (*b*) superimposed on the δ' unit cell in (*a*) with Li atoms in position B.

The preferred formation of configuration B can be explained by considering the bond energies among Al, Li and Cu atoms, either by comparing the Cu–Li and Cu–Al phase diagrams, or by examining the electronegativities of these elements. First, reference to the Cu–Li (Pelton 1986) and Cu–Al (Mondolfo 1979) phase diagrams shows that about 22 at.% Li is soluble in Cu at 190°C (the ageing temperature in this study), while only about 8 at.% Al is soluble in Cu at the same temperature. The higher solubility of Li in Cu than of Al in Cu indicates that the Cu–Li bond energy is significantly greater than that of Cu–Al, although these energies could not be accurately calculated because of limited thermodynamic data available for the Cu–Li system at 190°C. Comparison of the electronegativities for these elements gives a qualitative indication of the magnitude of the relative differences in bond energies. The electronegativities of Al, Cu and Li are 1·5, 1·9 and 1·0, respectively (Ralls, Courtney and Wulff 1976). Since an electronegativity difference of 1·7 is considered to approach an ionic bonding situation, there is a strong attraction between Cu and Li atoms where the electronegativity difference is 0·9, compared with Al and Cu or Al and Li where the electronegativity differences are 0·4 and 0·5, respectively. Therefore, it appears that the δ' phase grows on θ' with Li atoms adjacent to Cu atoms because of the strong attraction between Cu and Li atoms. Hence, in order to specify the orientation relationship completely between the δ' and θ' structures, the matching of Cu and Li atoms across the interface must be given.

The strong attraction between Cu and Li atoms also explains why APBs are observed for all the θ' precipitates in figs. 5 and 7. The θ' unit cell contains fourfold rotary-inversion axes parallel to the $\langle 001 \rangle$ direction passing through the corners of the cell. Because of this symmetry operation, Cu atoms on the top half of the unit cell are displaced from Cu atoms on the bottom half, i.e., Cu atoms on the left- and right-hand faces in the top half are displaced to the front and back faces on the bottom half of the unit cell, as seen from the unit cell in fig. 1 (*a*). When the two-phase precipitate forms by the growth of δ' with Li atoms across from Cu atoms, the rotary-inversion operation is preserved in the two-phase structure (symmetry is maximized); the δ' on opposite faces of the θ' plate are antiphase with respect to each other. This occurs for all integral numbers of unit cells, thereby explaining the APBs observed across all the θ' plates.

One interesting exception to this occurs in the region between the two parallel θ' plates labelled A in fig. 7 (*a*). In this area there does not appear to be an APB across the faces near the end of the four-unit-cell precipitate, although there is an APB across the faces outside of this region, as sketched in fig. 9. Since both sets of $\{100\}$ planes are not clear in the δ' near the end of the two-unit-cell precipitate, it is difficult to determine whether there is an APB in the δ'. However, it appears that on the opposite face of the four-unit-cell precipitate, an extra half-plane of atoms is present in the δ' at the position shown in fig. 9 and indicated by $\perp$ in fig. 7 (*a*). The reason why the four-unit-cell precipitate does not have an APB in region A is probably because this plate grew into the δ' phase pre-existing on the precipitate two unit cells thick.

3.4. *Edges of θ' precipitate plates*

Another feature of interest in fig. 7 (*a*) is that the $\{100\}$ planes appear to be continuous across the edges of the θ' plates, indicating that they are largely coherent with the matrix. Burgers circuits drawn around the plate edges fail to reveal the presence of any terminating planes at the edges. This supports previous suggestions (Dahmen and Westmacott 1983) that θ' plates can grow by the lateral migration of $(a/2)[100]$ and $(a/2)[010]$ partial dislocations with Burgers vectors parallel to the plate

Fig. 9

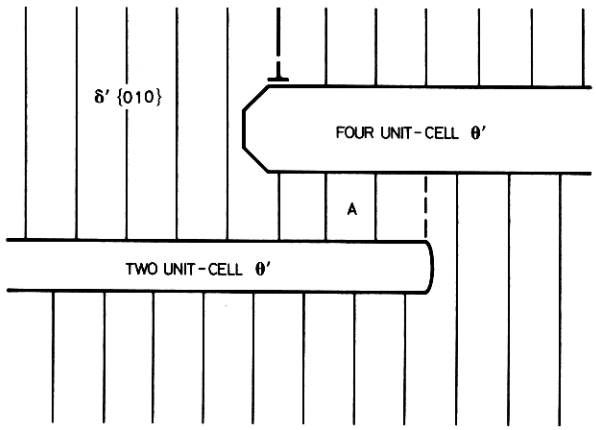

Illustration of the two- and four unit cell θ' plates in fig. 7(*a*) showing the positions of {100} planes and APBs across the precipitates.

faces, as opposed to perfect (*a*/2)[001] dislocations with Burgers vectors perpendicular to the faces and is analogous to the $\frac{1}{6}\langle 112\rangle$ Shockley partial dislocations which accomplish the f.c.c.→h.c.p. structural transformation required for growth of γ' plates on {111} planes in Al–Ag alloys (Nicholson and Nutting 1961, Hren and Thomas 1963, Howe, Aaronson and Gronsky 1985). It is also interesting to note that the θ'–δ' interface at the edge of the four unit cell θ' plate in fig. 7(*a*) is staggered at about 45° from the centre towards both faces, as sketched in fig. 9, rather than being flat as observed for most γ' precipitate plates in Al–Ag alloys (Howe and Gronsky 1986). This may be due to repulsion of (*a*/2)[100] and (*a*/2)[010] edge dislocations of the same sign as they approach the plate edge (Cottrell 1953).

The edge of the precipitate plate in fig. 3 is shown enlarged in fig. 10. Although the precise interface between the edge of the θ' plate and the δ' phase is not apparent because of overlapping of δ' and θ' through the foil thickness, it is possible to determine that the APB between δ' on either side of the θ' plate continues in the δ' past the plate edge, as evident from the mismatch of dark planes (arrows) in fig. 10. This indicates that the energy of the α–θ' interface at the plate edge is higher than the energy of a δ'–θ' interface with an accompanying APB in δ' since wetting of the plate edge with δ' occurs at the expense of creating an APB in the δ', or $\gamma_{\delta'-\theta'}+\gamma_{\mathrm{APB}}<\gamma_{\alpha-\theta'}$. Assuming that the energy of an APB in δ' is 0·175 J m^{-2} and that the energy of the δ'–θ' interface is similar to that of the δ'–β' interface in Zr-containing alloys at about 0·065 J m^{-2} (Gayle and VanderSande 1986) indicates that the interfacial energy at the θ' plate edge is probably at least 0·240 J m^{-2}. The δ' also appears to extend only about 1·6 nm beyond the edge of the θ' plate. The reason for this may be twofold:

(1) propagation of an APB in the δ' beyond the plate edge is energetically unfavourable, and this may restrict growth of the δ' phase much beyond the plate edge, and
(2) both the δ' and the θ' interfaces could be growing at nearly equivalent rates in the direction parallel to the plate faces because Li and Cu have similar diffusivities in Al at 190°C (Mondolfo 1979).

Fig. 10

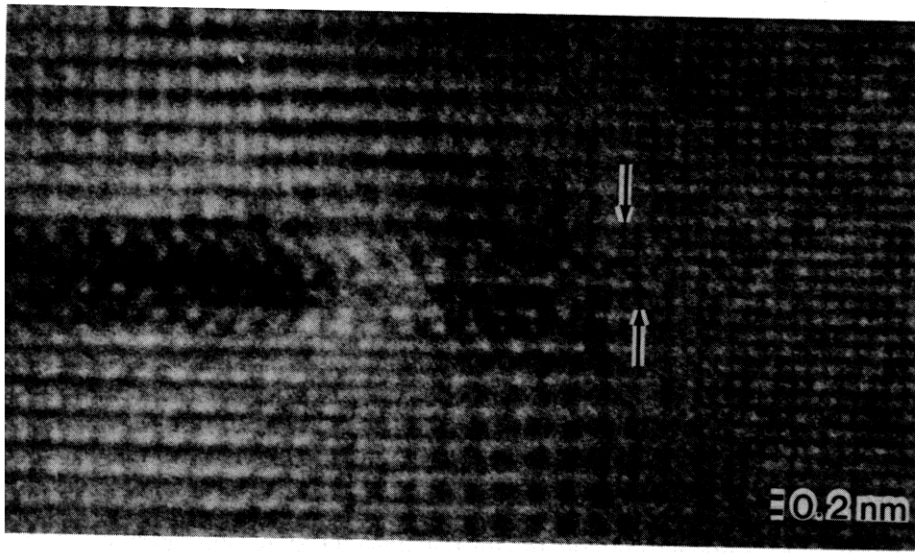

Enlargement of the θ' plate edge in fig. 3 showing propagation of an APB in the δ' phase (arrows) beyond the plate edge.

It is again interesting to note that the plate edge in fig. 10 is coherent with the δ' and α phases.

3.5. *Further discussion of δ' growth*

In § 1 it was mentioned that the formation of a two-phase precipitate structure is peculiar to Al alloys containing Li. The reason for this is now clear. The δ' phase has been found to envelop two phases in Al alloys, the θ' phase discussed here, and also the coherent Al_3Zr β' phase with an $L1_2$ structure, which forms when Zr is added to Al alloys containing Li. The common feature shared by θ' and β' is that they both have $\{001\}$ interfaces with exactly the same atomic arrangement as a $\{002\}$ plane in the δ' $L1_2$ structure (fig. 1). In addition, as discussed for the θ' structure above, the electronegative Cu atoms directly beneath the $\{001\}$ surfaces have exactly the same atomic arrangement as the electropositive Li atoms in the δ' structure, providing a further driving force for growth of δ' on θ'. In the case of β', there is only a 0·4 electronegativity difference between Zr and Li, but the pre-existing $L1_2$ arrangement of Zr and Al in the β' phase should catalyse nucleation of the $L1_2$ δ' structure, with Li atoms substituting for Zr atoms (Gayle and VanderSande 1986). Investigations using HRTEM are currently in progress to determine the arrangement of Li and Zr atoms across the β'–δ' interface in an Al–Li–Cu–Zr alloy to confirm this hypothesis (Kim, Howe and Boden 1987).

The δ' phase has not been observed to grow on other phases commonly found in Li-containing alloys, such as T_1 precipitate plates (Noble and Thompson 1972, Stimson *et al.* 1986) and the S′ phase in Al–Li–Cu(–Mg) alloys (Silcock 1960–61, Welpmann, Peters and Sanders 1986). The reason that δ' does not grow on either the T_1 or the S′ phases is that these precipitates do not have $\{001\}$ interfaces which resemble the $L1_2$ δ' structure. In addition, both T_1 and S′ are ternary phases with approximate stoichiometries of $Al_2Cu(Mg)Li$. In these intermetallics, the electropositive Li already

coexists with electronegative Cu and Mg, and there is a lower tendency for attraction of Li and nucleation of δ' in the adjacent matrix.

Lastly, the results of this study indicate that a significant portion of the δ' phase may grow epitaxially on the θ' precipitate plates, as supported by the following pieces of evidence. First, the ordered arrangement of Al and Li atoms in δ' coatings was observed to be unaltered along entire faces of θ' plates examined by HRTEM in this study, and the antiphase relation between δ' on opposite faces was also preserved across entire faces, out to the precipitate edges. Secondly, the fact that the δ' phase extends up to and slightly beyond the edges of θ' plates indicates that the θ' plates are immediately wetted by the δ' phase. Thirdly, further examination of the dark-field image in fig. 2 shows that an area denuded in δ' exists around many θ' plates. This may be partly due to preferential growth of δ' on θ', which depletes the surrounding matrix of Li. This evidence does not preclude the possibility that δ' precipitates may also nucleate and grow in the α matrix ahead of or nearby a growing θ' plate and impinge on the plate as it lengthens, and there is evidence that some of the δ' particles in fig. 2 may have joined the two-phase precipitates by impingement, such as the particle labelled D. In contrast, Tosten *et al.* (1988) have suggested that δ' precipitates nucleate before θ', independently in the α phase nearby, and that these phases grow together entirely by impingement rather than by epitaxial growth. *In situ* hot-stage TEM is being performed on δ'-reverted samples to distinguish between these two possible mechanisms of formation of the two-phase structure.

§4. Conclusions

This HRTEM study was performed in order to understand the reasons for the formation of a two-phase δ'–θ' precipitate structure in Al–Li–Cu alloys. The results from this investigation show the following.

(1) The θ' phase grows in integral numbers of unit cells in Al–Li–Cu alloys, as opposed to combinations of integral and fractional numbers of unit cells in Al–Cu alloys.
(2) The δ' phase in the two-phase structure grows epitaxially on the θ' plates owing to the similar arrangement and strong attraction between Cu and Li atoms in the two structures.
(3) An antiphase relation occurs between the δ' phase on opposite faces of θ' plates because of the attraction between Cu and Li atoms in the θ' and δ' phases and the location of the fourfold rotary-inversion axes in the θ' unit cell.
(4) The antiphase relationship between the δ' that forms on opposite faces of θ' plates is retained after the δ' propagates past the edges. This forms an APB and the δ' coating at the edges is at least an order of magnitude less thick on the faces after significant development of the two-phase structure.
(5) The edges of θ' plates are largely coherent with the surrounding δ' and α matrix, indicating the possibility of growth by $(a/2)[100]$ and $(a/2)[010]$ partial dislocation ledges rather than $(a/2)[001]$ prismatic dislocations.

Acknowledgments

This work was supported by grants from Alcoa (A.K.V., J.M.H. and D.E.L.), Carnegie Mellon University (J.M.H.) and the National Science Foundation under Contracts DMR-8610439 (J.M.H.) and DMR-8413115 (D.E.L.).

References

BAKER, C., GREGSON, P. J., HARRIS, S. J., and PEEL, C. J., 1986, *Aluminium–Lithium Alloys III* (London: Institute of Metals).

COTTRELL, A. H., 1953, *Dislocations and Plastic Flow in Crystals* (Oxford University Press), p. 48.

COWLEY, J. M., and MOODIE, A. F., 1957, *Acta crystallogr.*, **10**, 609.

DAHMEN, U., and WESTMACOTT, K. H., 1983, *Phys. Stat. Sol.* (a), **80**, 249.

GAYLE, F. W., and VANDERSANDE, J. B., 1986, *Aluminium–Lithium Alloys III* (London: Institute of Metals), p. 376.

GLAZER, J., EDGECUMBE, T. S., and MORRIS, J. W., JR, 1986, *Aluminium–Lithium Alloys III* (London: Institute of Metals), p. 369.

HREN, J. A., and THOMAS, G., 1963, *Trans. metall. Soc. A.I.M.E.*, **227**, 308.

HIRSCH, SIR, P., HOWIE, A., NICHOLSON, R. B., PASHLEY, D. W., and WHELAN, M. J., 1977, *Electron Microscopy of Thin Crystals* (Malabar, Florida: R. E. Krieger), p. 505.

HOWE, J. M., and VASUDÉVAN, A. K., 1988, *Metall. Trans. A* (to be submitted).

HOWE, J. M., AARONSON, H. I., and GRONSKY, R., 1985, *Acta metall.*, **33**, 639, 649.

HOWE, J. M., and GRONSKY, R., 1986, *Materials Problem Solving with the Transmission Electron Microscope* (Pittsburgh, Pennsylvania: Materials Research Society), p. 241.

HUANG, J. C., and ARDELL, A. J., 1986, *Aluminium–Lithium Alloys III* (London: Institute of Metals), p. 455.

KIM, N. J., HOWE, J. M., and BODEN, E. G., 1987, *J. Phys., Paris*, **48**, C3–457.

MONDOLFO, L. M., 1979, *Aluminium Alloys: Structure and Properties* (London: Butterworths), p. 253.

NICHOLSON, R. B., and NUTTING, J., 1961, *Acta metall.*, **227**, 332.

NOBLE, B., and THOMPSON, G. E., 1971, *Metal Sci. J.*, **5**, 114; 1972, *Ibid.*, **6**, 167.

O'KEEFE, M. A., 1984, *Proceedings of the Third Pfeffercorn Conference, Ocean City, Maryland* (Chicago, Illinois: SEM, Inc.), p. 209.

O'KEEFE, M. A., and BUSECK, P. R., 1979, *Trans. Am. Cryst. Assoc.*, **15**, 27.

PELTON, A. D., 1986, *Bulletin Alloy Phase Diagrams*, **7**, 142.

RALLS, K. M., COURTNEY, T. H., and WULFF, J., 1976, *Introduction to Materials Science and Engineering* (New York: Wiley), p. 54.

RIOJA, R. J., and LUDWICZAK, E. A., 1986, *Aluminium–Lithium Alloys III* (Warrendale, Pennsylvania: Metallurgical Society of AIME), p. 471.

SANDERS, T. H., and STARKE, E. A. JR (editors), 1981, *Aluminium–Lithium Alloys* (Warrendale, Pennsylvania: Metallurgical Society of AIME); 1984, *Aluminium–Lithium Alloys II* (Warrendale, Pennsylvania: Metallurgical Society of AIME).

SILCOCK, J. M., 1959–60, *J. Inst. Metals*, **88**, 357; 1960–61, *Ibid.*, **89**, 203.

SILCOCK, J. M., HEAL, T. J., and HARDY, H. K., 1953–54, *J. Inst. Metals*, **82**, 239.

SPENCE, J. C. H., 1981, *Experimental High-Resolution Electron Microscopy* (Oxford: Clarendon), p. 85.

STIMSON, W., TOSTEN, M. H., HOWELL, P. R., and WILLIAMS, D. B., 1986, *Aluminium–Lithium Alloys III* (Warrendale, Pennsylvania: Metallurgical Society of AIME), p. 386.

STOBBS, W. M., and PURDY, G. R., 1978, *Acta metall.*, **26**, 1069.

TOSTEN, M. H., VASUDÉVAN, A. K., and HOWELL, P. R., 1988, *Aluminium–Lithium Alloys III* (Warrendale, Pennsylvania: Metallurgical Society of AIME), p. 483.

TOSTEN, M. H., VASUDÉVAN, A. K., and HOWELL, P. R., 1988, *Metall. Trans.* A, **19**, 51.

WELPMANN, K., PETERS, M., and SANDERS T. H., JR., 1986, *Aluminium–Lithium Alloys III* (Warrendale, Pennsylvania: Metallurgical Society of AIME), p. 524.

WILLIAMS, D. B., and HOWELL, P. R., 1988, *Modern Aluminium Alloys* (New York: Academic Press) (to be published).